Small-world networks of neuroblastoma cells cultured in three-dimensional polymeric scaffolds featuring multi-scale roughness

Onesto Valentina, Angelo Accardo, Christophe Vieu, Gentile Francisco

Small-world networks of neuroblastoma cells cultured in three-dimensional polymeric scaffolds featuring multi-scale roughness

Valentina Onesto[1,*], Angelo Accardo[2,#,*], Christophe Vieu [2,3,†], Francesco Gentile[4,†]

[1] Center for Advanced Biomaterials for Healthcare, Italian Institute of Technology, Naples, Italy

[2] LAAS-CNRS, Université de Toulouse, CNRS, F-31400, Toulouse, France

[3] Institut National des Sciences Appliquées – INSA, F-31400 Toulouse, France

[4] Department of Electric Engineering and Information Technology, University Federico II, 80125 Naples, Italy

* these authors contributed equally to the work

† these authors share senior authorship

[#] Current Institute: Department of Precision and Microsystems Engineering, Delft University of Technology, Mekelweg 2, 2628 CD Delft, The Netherlands

Understanding the mechanisms underlying cell-surface interaction is of fundamental importance for the rational design of scaffolds aiming at tissue engineering, tissue repair and neural regeneration applications. Here, we examined patterns of neuroblastoma cells cultured in three-dimensional polymeric scaffolds obtained by two-photon lithography. Because of the intrinsic resolution of the technique, the micrometric cylinders composing the scaffold have a lateral step size of $\sim 200\ nm$, a surface roughness of around $20\ nm$, and large values of fractal dimension approaching 2.7. We found that cells in the scaffold assemble into separate groups with many elements per group. After cell wiring, we found that resulting networks exhibit high clustering, small path lengths, and small world characteristics. These values of the topological characteristics of the network can potentially enhance the quality, quantity and density of information transported in the network compared to equivalent random graphs of the same size. This is one of the first direct observations of cells developing into $3D$ small world networks in an artificial matrix.

Keywords: small world networks, 3D networks, neuro regeneration, tissue engineering, two photon lithography, biomaterials

1. Background

In tissues and organs, and especially the brain, the interaction between a large number of cells determines the emergence of functions that are not explicable in terms of individual cells taken individually [1-9]. In similar systems, organization, communication, and cooperation between elements are decisive for the correct functioning and optimal performance of the systems themselves. Network theory is a practical way to examine biological systems on a quantitative basis [10-14]. Networks are groups of nodes (or vertices) and edges (or links) that connect those nodes – in which the nodes represent the elements of the systems and the edges the interactions between them [15-18]. Networks can be described through three sole parameters. The degree of a network k is the average number of links per node. The local clustering coefficient cc_l of a node is the proportion of active established links to the number of possible connections in the neighborhood of that node (the global clustering coefficient cc is determined by averaging cc_l over the nodes of the network). The characteristic path length cpl is the average number of steps that separate two nodes randomly chosen in the grid [15-18]. Among the great variety of network categories with different features, *small world* networks have recently attracted attention because it is believed that networks with small world attributes can transmit signals (or instructions) more efficiently than periodic or unstructured graphs of the same size [19-23]. For the same reason, a system with a small world architecture can divide tasks between its components, coordinate activities, and optimize processes more efficiently than ordinary systems without structure. In a small world network, the distance (i.e. cpl) between the elements of the network raises less rapidly than its size (N), such that $cpl \sim log(N)$: this indirectly implies that – typically – nodes of the network form few, highly connected clusters, with short paths between them [19-23]. In such context, materials science combined with nanofabrication methods provide ways to drive the organization of living cells into artificial structures engineered according to a desired design. In previous works, some of the authors of this paper have shown that cells, cultured on nano-patterned surfaces, evolve to form networks with small world characteristics, where the nano-scale roughness of the substrate represents the external factor that forces the cells to collapse into energetically favorable configurations[7]. A similar behavior has been observed for neuroblastoma cells on mesoporous silicon substrates [24], as wells as for neuronal cells on rough silicon substrates [7] and arrays of zinc oxide nanowires [25]. Nonetheless, these results are limited to bi-dimensional geometries.

Here, we examined the topology of $3D$ networks of neuroblastoma cells cultured in polymeric scaffolds fabricated by two-photon lithography, focusing on the data reported in reference [26]. Due to the fabrication process characteristics, the scaffold presents topography details over multiple scales: the micrometer-scaled cylinders of the scaffold have been patterned with a lateral step size of $\sim 200\ nm$ that, in turn, results in a surface roughness of $\sim 20\ nm$. Upon networks analysis, we found that cells form small world networks, with higher clustering and smaller paths than in equivalent random graphs with the same size: the hierarchical structure of the scaffold being the possible cause of cell response. This is one of the first direct observations of cells developing into $3D$ small world networks in an artificial matrix.

This study was not focused on optimizing performance nor examining in detail all the possible combinations of geometrical characteristics of the scaffold, mechanical properties, surface functionalization, cell lines characteristics, that may affect cell behavior. The main objective of this preliminary study was to demonstrate the feasibility of using network analysis and the small-world-network model to describe the spatial organization of mammalian cells in 3D architectures. Data presented in the paper and analysis thereof represent a preliminary reference for future studies. More sophisticated test campaigns that will be performed over time will verify the combined effect of geometry, nano-topography, mechanical properties of the scaffold on the collective behavior and self-assembly of primary hippocampal neurons, that are more representative of the central nervous systems.

2. Results

2.1 Three-dimensional polymeric scaffolds. The scaffolds where cells were seeded is an ordered network of polymeric cylinders (**Figure 1a**), with a diameter $D = 20\ \mu m$, and a spacing between structures of $d_1 = 20\ \mu m$ and $d_2 = 60\ \mu m$ in the vertical and horizontal direction, respectively (**Figure 1b**). The entire scaffold is embedded within a cube with edge length of $l = 300\ \mu m$. While the overall volume of the scaffold is such to contain a sufficiently high number of cells, the openings within the scaffold enable cells to develop without geometrical constraints. SEM inspection of the scaffold reveals that, due to the fabrication process resolution (methods), the final structures are discretized into smaller blocks with a lateral step size of $s \sim 200\ nm$ (**Figure 1c**). 2D photo polymerization of structures with similar values of lateral step size results, generally, in a surface roughness that is not zero. The surface roughness R_a can be

estimated by previous works[27], where R_a has determined as a function of the lateral step size of three dimensional polymerized structures. For the present configuration R_a is estimated as $R_a \sim 20\ nm$[27]. Structures in the scaffold have therefore a multiscale roughness and details organized in a hierarchical architecture, from the micro scale level (cylinder size) to the high (lateral step size) and low (surface roughness) nano meter range. We have generated in **Figure 1d** the surface state of a cylinder with a similar structure and, by Fourier analysis of the surface topography[28], we have derived the Power Spectrum (PS) density function of the scaffold (**Figure 1e**). The PS describes how the information content of an image (Q) varies as a function of its spatial frequency (ν) – it reports a change of density (of information) as a change of scale. Therefore, the slope β of a PS can be correlated to the fractal dimension D_f of a structure as[28] $D_f = (8 - \beta)/2$. For the present configuration, it results $D_f \sim 2.7$. Moderate values of surface roughness ($R_a \sim 20\ nm$) and high values of fractal dimension ($D_f \sim 2.7$) are agents that may force cells to cluster into few groups, with many elements per group, as previously reported for 2D geometries[7,24,25].

As regarding the mechanical features of the scaffold: the hierarchical structure was fabricated from liquid polymer, i.e. the negative photoresist IP-Dip. Nanomechanical characterization of IP-Dip[29] yielded for this material the following values of average Young's modulus $\mathrm{E} = 2.1 \pm 0.3$ GPa and an average yield strength under compressive loads $\sigma_y = 67.2 \pm 4.7$ MPa. Nevertheless, experimental measurements of the effective Young modulus E eff of periodic lattices governed by bending effects was found to scale as $\mathrm{E_{eff}} = \mathrm{E_s}\ \rho^2$, where $\mathrm{E_s}$ is the bulk Young modulus of the constitutive material (IP-Dip), ρ the relative density of the scaffold[30]. Our scaffold exhibits a relative density close to 20%. This gives an effective young modulus of the produced scaffold $\mathrm{E_s} \sim 80\ MPa$. N2A cells thus contact a stiff material (IP-Dip) of young modulus in the GPa range, but they are embedded inside a deformable scaffold of effective stiffness around 80 MPa. Remarkably, the stiffness found for IP-Dip is, even considering the reduction in the strength of E due to the lattice geometry, ~ 40 times larger than the average Young's modulus of PDMS ($\mathrm{E} = 2 \pm 0.1$ MPa), that has been used in previously reported experiments[31] to determine the average traction forces exerted by differentiated Madin-Darby canine kidney (MDCK) epithelial cells on a substrate, being approximately $\mathrm{F} \sim 2\mathrm{nN}/\mu m^2$. This, in turn, implies that the deformation of the scaffold caused by N2A cells is – for this configuration – negligible,

and the behavior of cells and the characteristics of the networks that they form can be ascribed to *geometry* solely.

2.2 Cell distribution. Neuroblastoma N2A cells were seeded in the scaffolds using the protocols described in the Methods. Then, cells were imaged 3 days after seeding using light sheet microscopy and two photon confocal microscopy as described in reference [26]. N2A cells were not differentiated – i.e. no differentiation medium or methods were employed at any point of study. Light sheet microscopy enables qualitative analysis of the cells (**Figure 2a**), that appear unevenly distributed within the entire volume of the scaffold (here represented as a cube with an edge of $l{\sim}300\ \mu m$). SEM analysis reveals that cells preferentially align along the nanometric grooves of the scaffold (**Figure 2b**), that therefore exert significant influence over the cell behavior. Surface roughness of the scaffold, organized over different dimensional scales, seem to cause cells to precipitate into aggregates (**Figure 2c**). Two photon confocal microscopy was employed to obtain quantitative localization of individual cells within the scaffold. The total number of cells in the volume of interest is $N = 233$. Using a 3D scatter plot representation of the cells (**Figure 3a**), with the z axis aligned along the vertical edge of the scaffold, one can observe that cells are preferentially distributed around the upper (high $z's$) and lower (small $z's$) parts of the scaffold (**Figure 3 b-c**), and generally along its perimeter (**Figure 3d**). This is also evidenced by rotating clockwise the scatter plot of cells through successive angles θ around the z axis, with $\theta = (0 - \pi)$ (**Supporting Information Figure 1.1**), that provides complete vision of the cell distribution within the three-dimensional volume. We then projected the positions of the center of the cells, initially distributed over the entire volume of the scaffold, on the three orthogonal planes xy, xz, yz. This enabled to derive the quantitative profile of cell distribution in the plane that were in turn projected along the edges of the cube to obtain the frequency distributions f along the x, y and z directions (**Figure 4**). From the distributions, one can notice that f is non uniform over the planes of projection and along the principal directions of the scaffold, with the number of cells per line micrometer varying between a minimum of $f{\sim}0.2\ \ cells/\mu m$ and a maximum of $f{\sim}1.2\ \ cells/\mu m$, with a more than six times increase. Notice that the integral of the $f's$ over the edge of the cube is 233, i.e. the number of cells contained in the scaffold.

2.3 Cluster analysis of cells. We performed unsupervised cluster analysis of cells to examine whether a non-uniform cell distribution results in the emergence of separate groups in the scaffold. We used a density based clustering algorithm, originally developed by Rodriguez and Laio

in 2014[32], to determine cluster centers as those cells in the set with higher density than their neighbors and by a relatively large distance from cells with higher densities (methods). From the analysis (**Figure 5a**) it results that there are at least 7 separate cluster centers in the original set, as reported in **Figure 5b**. The remaining cells are then assigned to specific clusters on the basis of their Euclidian distance to the clusters. In **Figure 5c** cells are colored according to the cluster to which they are assigned. The discovery of a finite number of sub-groups in the cell distribution suggests that cells can form networks with high clustering and short paths.

2.4 Network analysis of cells. The two-photon confocal imaging technique used in reference [26] enabled to determine the position of the cells in the scaffold but not their connections. We used the Waxman algorithm[33] to create, artificially, the topological networks associated to the coordinates of neuroblastoma cells in the space. The Waxman algorithm makes a decision on whether couples of cells are connected or not, based on their distance. It states that the probability p of two nodes (u, v) of being connected is:

$$p(u,v) = \alpha e^{-d(u,v)/\beta l} \quad (1)$$

where $d(u,v)$ is the Euclidean distance between u and v, l is the maximum distance between pairs of nodes, and α and β are parameters of the model that are here set as $\alpha = 1$, β =0.1 (**Supporting Information 2**). Thus, the larger the distance between two cells, the smaller p. By comparing p to an arbitrary threshold probability $P = 1 - q$, one can decide if nodes establish a connection ($p > P$) or not ($p < P$). We used different values of q and P ($q = 0.7 - 0.95 \rightarrow P = 0.3 - 0.05$) to construct the topological graphs associated to the real biological prototype (**Figure 6**). The larger q (the smaller P) the denser the graphs, in the limiting case $q = 1$ nodes of the graph establish all possible connections between them, producing a complete graph (at the opposite extreme, $q = 0$, the graph is null, with no connections between nodes).

We then computed the graphs parameters using the algorithms reported in reference [7] and the methods. For specific values of q (**Figure 7a**) we determined the degree of the graph k, the clustering coefficient cc, the characteristic path length cpl, the small world coefficient SW (**Figure 7b-e**). The graph parameters exhibit a very high sensitivity to q. The degree of the network k varies between $k \sim 3$ for $q = 0.7$ and $k \sim 16$ for $q = 0.95$ (**Figure 7b**). The degree of a network represents the average number of connections per node, i.e. the number of synapses per neuron in a biological interpretation of the results.

Even if N2A cells cannot differentiate into fully functional neurons, still they can develop multiple neuritic connections per single cell, although rarely more than 5, and each connection can develop sub-branches which may or may not link with other cells. In previous experimental reports, it has been observed that the number of neuritic extensions per N2A cell varies from approximately $2-3$ for un-patterned SiO_2[34], to around 3 for free-standing PEGDA hydrogel architectures[35], to $3-5$ for surfaces patterned with arrays of carbon nanotubes[34]. Numbers of neuritic extension/cell greater than 5 are observed with lower probability values.

On modulating q between the considered interval, resulting values of k oscillate around the characteristic value $k=4$, stretching below and above it. This choice of $q's$ is thus founded on a biological basis. The maximum theoretical value of $k=16$, while significantly larger than the maximum determined number of neuritic extension per cell, ~ 5, still is sufficiently large to cover possible cases in which, owing to specific conditions and geometries, the number of neuritic extensions that cells develop rises above the limits heretofore registered.

Best fit of data and graphical representation of $k(q)$ indicate that k is a cubic function of q: $k=-571+2240\,q-2928\,q^2+1286\,q^3$, perhaps indicating the fact that the network is immersed in a $3D$ −space and, for a variation in q (i.e. the probability of connectivity), the nodes of the systems tend to create new connections along 3 independent directions. We calculate a r-squared statistic r^2 to test whether the data in several different bands are consistent with the matching template. Values of r^2 near unity and of estimated variance σ^2 near zero indicate that the signal is consistent with the model ($r^2\sim 0.997$, $\sigma^2\sim 0.04$).

Differently from k, and with the exception of the first ($q=0.7$) and last ($q=0.95$) values of q, the clustering coefficient shows a low sensitivity to q, with values of cc oscillating around the average ($cc\sim 0.71$), and in any case greater than $cc\sim 0.70$ (**Figure 7c**). Recalling that the clustering coefficient varies between 0 and 1, in the considered range of $q's$, the cells of the network exhibit a very high inclination to cluster together. *Vice versa*, in the same domain of variation for q, the characteristic path length cpl of the network is generally *low*, the number of steps separating two nodes of the graph being smaller than 3.5 for each considered configuration (**Figure 7d**). Combined together, the clustering coefficient cc and the characteristic path length cpl enable to determine the small-world coefficient of a graph. We used the topological measure *small-worldness* SW, defined in reference [36] and the methods to examine whether cultured cell graphs exhibit *small world* attributes. Calculated values of SW range between SW$\sim$1 and SW$\sim$1.4 for $q>$

0.72, while SW∼0.85 for $q = 0.70$ (**Figure 7e**). For the large majority of the considered possible values of q the graphs surpass the small-worldness test (SW values are greater than one) and, analyzing their degree distribution, for large κ the probability of finding a highly connected vertex decreases exponentially with κ (power-lawness test was negative – **Supporting Information 3**), therefore we are confident to claim that these networks obey a small-world configuration[37].

3. Discussion

The central and peripheral nervous system could be seen as a very large array of computational units linked together in a structure with some degree of order. The organization of the brain affects, in turn its efficiency, and its ability to performing tasks – such as image and speech recognition, object classification, unstructured problem-solving – that are inherently difficult in conventional Von Neumann architectures, on which much of modern computers are based. In Von Neumann architectures, a core logic operates sequentially on data fetched from memory. In contrast, biological computing distributes both computation and memory among an enormous number of relatively simple neurons, each communicating with hundreds or thousands of other neurons through synapses. The spatial distribution of neurons over hierarchal scales is the factor that may possibly explain the enhanced computational power, increased versatility, and reduced low energy consumption of neuromorphic systems compared to the von Neumann chips. Many scientists are skeptical about the idea of the brain as a computer, representing an oversimplification of an intrinsically irreducible problem. The cognitive processes underpinning human language and consciousness, intuition and creativity, are perhaps excessively complex to be decomposed into a sequence of more fundamental instructions, or a list of causes and effects. Nevertheless, this view is of some utility if one wants to analyze the nervous system mathematically, and translate problems of the neuroscience into tractable mathematical formulations, which may provide insight into the originating application. In representing the brain as a network of logic gates (the neurons), one can study the nervous systems, or some of its parts, using the methods and the variables typical of topological theories and the theory of information, including the clustering coefficient, the characteristic path length, the small world coefficient, and the Shannon information entropy[21,38,39].

Results of the paper indicate that N2A nerve cells in 3D geometries evolve to form networks with small world characteristics. In other words, in a cascade of biological processes, including adhesion and migration, cells transit from an initial, random, configuration to a structure with a strong correlation between its internal parts. The high values ($SW > 1$) of the small world coefficient being indicative of such a correlation. Thus, evolution shapes an ensemble of relatively simple elements into a structure that (because of specific topologies) can more efficiently and more rapidly elaborate and transmit information: that is the own function of the brain. While nerve cells are genetically programmed to form similar information-efficient structures, still they may be restricted to do this, unless they are not fueled by a proper external force. In artificial scaffolds that support cell growth and proliferation, this force is generated by the surface roughness, organized on hierarchical levels, that at the single cell level is in the order of some tens of nanometers – similarly to what precedently observed for bi-dimensional geometries [7,24,25]. Multi scale nano-topography is the endogenous factor that sets off cell condensation. Understanding how surface topography, cell network topology and information are interconnected, is of fundamental importance in the design of scaffolds for neuronal tissue engineering and neuro-regenerative medicine, where the ultimate goal is replacing, engineering or regenerating nerve cells to restore the normal functions of the cells themselves, i.e. elaborate information.

The networks that we analyzed are the results of a numerical rewiring of the positions of cells tracked with two photon confocal microscopy techniques. They are not a representation of a real neuronal network, but are partly based on an estimate on how N2A cells may form connections if placed on specific points of the scaffold determined by experiments. The Waxman algorithm that we used to model cell connections is based on the assumption that the strength of a connection decays exponentially with cell-cell distance, that is a reasonable hypothesis validated by independent observations[38,40], and on three model parameters, i.e. α, β, q. The choice that we made on α, β, q was not arbitrary: α and β were chosen to maximize the sensitivity of the probability of connection to the cell-cell distance, while q was tuned to modulate the average number of connections per node in the resulting networks. In the array of different configurations that we obtained by changing q, the number of connections per node varies from $k\sim3$ to $k\sim16$. Calculated values of SW are greater than one for each of the configurations in this interval, indicating that results presented in the paper are general in nature and robust to a change in the model parameters. Values of k outside this interval were not considered (i) either because resulting net-

works are excessively sparse ($k < 3$) or (ii) because k would is excessively higher the number of connections-per-cell normally found in N2A systems, that is around $3 - 4$ ($k > 16$). The neuroblastoma N2A cells model that we used in this study is a simplified version of primary neuronal cultures. Compared to these, N2A cells do not form as many neuritic extensions and cannot generate mature neurites. Nevertheless, among the characteristics found in N2A there are: the expression of neuro-filaments, the synthesis of neurotransmitter biosynthetic enzymes, differentiation, the elaboration of neuritic processes that are ultra-structurally and electro-physiologically similar to normal neurons[41]. The evolution and development of N2A cells in a conditioned system can therefore approximate and reflect some of the most salient features and biologically relevant aspects of primary neurons in the same system. Results of this simplified experimental model, while they represent a preliminary reference for the study of the organization of neuronal cells in three dimensional architectures, have to be investigated even further with additional experiments with primary neuronal cells and tissues in even more complex geometries. Some of these experiments may involve the reconstruction of the real connections formed in groups of neurons with techniques as those described, for example, in references[42,43], to achieve maximum adherence of the model to the real physical prototype.

In more sophisticated experiments that will be performed over time, we will assess cell connectivity in networks of *primary neuronal cells*, and will verify to which extent the small-world-network analogy is relevant in systems of neurons developing multiple, free standing neuritic connections, in rigid as well as in *soft* materials, where the contribution of scaffold deformations cannot be neglected[35].

Similarly, we will design an experimental campaign to verify the effects of *drugs* (chemotherapeutic agents or other therapeutic agents) on the 3D/spatial organization of N2A cells, neuronal cells, or other cell lines. We will verify whether and to which extent the delivery of therapeutics and the nano-topography on the scaffold surface combine to facilitate *or* prevent cell adhesion, proliferation, and networking. More importantly than this: we will examine whether the physiological/pathological conditions of cell and of a system of cells may be reflected by the topological parameters of that system. May the clustering coefficient, the characteristic path length, and a combination of these, quantitatively reflect the health status of systems of cells, i.e. organs, tissues, organoids?

Lastly, since the role of the glial cells cannot be neglected (using recently validated isotropic fractionator, it has been observed that in the brain the glia:neuron ratio is about 1: 1, with a total number of less than 100 billion glial cells in the human brain[44]), we will design experiments to examine whether co-cultures of neurons/glial cells may affect cell networking.

4. Conclusions

Results of the paper indicate that cells in 3D scaffolds form non-homogeneous, non-uniform systems, with cells forming few groups with a great many of elements per group. Cells used in this study are neuroblastoma N2A cells. While they share most of the characteristics of primary neuronal cells (cfr. the Discussion of the paper) and give a preliminary indication of the evolution of a system of nerve cells under the influence of surface nano-topography, nonetheless additional experiments with primary neurons are needed to examine the phenomenon on a more rigorous basis. The small-world-network model implemented in the paper describes convincingly the topology of the clusters of cells in the scaffold. Since small-world networks are theoretically believed to receive, elaborate, and transmit information (i.e. signals) more efficiently than equivalent random or periodic networks of the same size, this also suggests that the main drivers for nerve cell condensation are *energy minimization* and *information maximization*, these two criteria being perhaps equivalent. That is to say – biological systems of cells are shaped by evolution to keep the energy of the system at a minimum and, *simultaneously*, the information exchanged in the system at a maximum. Optimization of these *cost functions* would, to cite a few, explain the low energy consumption of the brain and the formation in the cerebral cortex of structures with a finite size like the cortical mini-columns, that are the basic computational units of the brain. The nano-topographical details that decorate the surface are the factors that trigger cell condensation in artificial scaffolds. Understanding the role of cell topology and surface nano-topography on the organization of nerve cells into complex structure may help to design strategies for tissue engineering, nerve repair, neuronal regeneration, faster and more efficiently.

5. Methods

5.1 Fabrication of the polymeric scaffolds. Briefly, the 3D scaffolds were fabricated by exploiting a two-photon direct laser writing approach where the slicing (minimal distance between two adjacent planes) and hatching (lateral distance of two adjacent lines within a layer) distances were set at 300 and 200 nm, respectively. Further details of the fabrication configuration can be found elsewhere[26].

5.2 SEM imaging images of the samples. SEM imaging was performed on the samples (metal-coated with 15 nm of sputtered gold) by using a Hitachi S-4800 microscope with an acceleration voltage ranging from 0.8 to 15 kV.

5.3 Culturing mouse neuroblastoma N2A cells in the scaffold. Prior to cell culture, the 3D scaffold was first sterilized for 1 h under UV (254 nm), then coated with 0.01% poly-l-lysine (Sigma-Aldrich), to favor the electrostatic interactions between the negatively charged ions of the cellular membrane and the employed polymer, washed twice with sterile water and dried for 2 h. Then, laminin (a protein of the extracellular matrix, involved as well in the mechanisms of cell adhesion) solution (40 $\mu g/ml$, Invitrogen) was applied for 3 h. The fast-growing mouse neuroblastoma cell line, N2A, was obtained from the American type culture collection. Dulbecco's modified Eagle's medium (DMEM) containing glutamax, pyruvate (Dubco, Invitrogen) and 10% fetal bovine serum was used for the N2A cells. 100,000 cells/cm^2 were inoculated onto the scaffold and left in culture for 3 days in vitro. Cells were incubated in an atmosphere containing 5% CO_2 at 37 °C.

5.4 Two-photon confocal imaging of cells in the scaffolds. The two-photon confocal imaging experiments were performed using an AxioImager upright microscope LSM 7MP (Carl Zeiss). Z-stack acquisitions were performed with a 20 × W-Plan Apochromat water immersion objective with 1.0 N.A., with the laser excitation wavelength tuned to 820 nm, giving a resolution on the x/y-axis of 430 nm and on the z-axis of 1.3 μm. Further details of the imaging configuration can be found elsewhere[26].

5.5 Cluster analysis. Cluster centers were determined using a density based clustering algorithm reported in reference[32]. The algorithm determines the number of groups into which the elements of the set are partitioned, and assigns each element to a group. The algorithm classifies elements into categories on the basis of their similarity. Cluster centers are determined as those points in

the set with higher density than their neighbors and by a relatively large distance from points with higher densities. For each cell i in the original distribution, the algorithm:

(i) Determines the density of i, $\rho(i)$, as the number of points that falls within a cut off distance δ_{co} from i, divided by the total number of points in the set.

(ii) Finds the subset $s \, \epsilon \, S$ of points in the dataset with densities $\rho(s) > \rho(i)$.

(iii) Finds the point $a \, \epsilon \, S$ with minimum distance to i, this distance is $\delta_{min/\rho}(i)$: the minimum distance of i from points with higher densities than i.

(iv) Derives a diagram where the density ρ is reported against $\delta_{min/\rho}$ per each element in the data set. Points in the set with higher density than their neighbors and by a relatively large distance from points with higher densities emerge as singularities in the diagram, an example of which is reported in **Figure 4**. These points are the cluster centers.

(v) Assigns each point in the set to different clusters on the basis a minimum distance criterion: a point b is assigned to a cluster G_i if the minimum distance of b to G_i is the smaller among all the minimum distances calculated with the remaining clusters. Thus clusters are constructed per accumulation. The cluster centers represent the seeds of the clusters. In **Figure 4**, points are colored according to the cluster of group to which they are assigned.

5.6 Wiring cells to form networks: the Waxman algorithm adapted to $3D$ spaces. In order to establish the nodes connections, we first need to derive the distance between the nodes. Being each node in the network described by three coordinates (x, y, z), the *distance matrix d* is obtained calculating the Euclidean distance between each node pair in the 3D space. If there are n elements in the network, the *distance matrix* is a symmetric two-dimensional array having size nxn. No matter how many dimensions we have in a Euclidean space, once derived the *distance matrix*, the calculation of the nodes connections is the same of the case of the 2D spaces. The Waxman model[33] is used to establish the connections between the nodes, whereby the probability of being a link between two nodes exponentially decreases with the Euclidean distance *d* between those nodes. For a given set of two nodes *u* and *v*, the link probability, $P(u, v)$ is defined as:

$$P(u, v) = \alpha e^{-d(u,v)/\beta l} \quad (2)$$

where l is the largest possible Euclidean distance between two nodes of the grid. In the equation, α and β are the Waxman model parameters and, upon tuning these, the graph may be more or less dense. α and β should be chosen between 0 and 1. Selecting smaller values of these parameters results in a smaller number of links. For the present configuration, these parameters were set to $\alpha = 1$ and $\beta = 0.1$. The probability *P* varies between 0 for a pair of nodes with an ideally infinite distance, and 1 for a pair of nodes with an ideally zero distance. The information about the connections among the nodes in a graph is contained in the *adjacency matrix* $A = a_{ij}$, where the indices i and j run through the number of nodes n in the graph; $a_{ij} = 1$, if there exists a connection between i and j, $a_{ij} = 0$ otherwise. In the analysis, reciprocity between nodes is assumed, and thus if information can flow from i to j, it can reversely flow from j to i. In the framework of graph theory, we call a similar network an undirected graph. Notice that this property translates into symmetry of A being $a_{ij} = a_{ji}$. We showed above how to derive the distances between nodes d_{ij} in the networks. On the basis of d, we may decide whether a pair of nodes is connected, we use at this end the formula:

$$\alpha e^{-d_{i,j}/\beta L} - P \geq 0 \tag{3}$$

in which P is a constant that we have chosen being between $0.3 - 0.1$ that the probability of being a connection is $q = 1 - P = 0.7 - 0.9$.

5.7 Network analysis of 3*D* graphs. We quantified some network parameters including the *clustering coefficient*,the *characteristic path length* and the *small-world-ness*. In graph theory, the *clustering coefficient* (C_c) is a measure of the degree to which nodes in a graph tend to cluster together. C_c ranges from 0 (none of the possible connections among the nodes are realized) to 1 (all possible connections are realized and nodes group together to form a single aggregate). The clustering coefficient is defined as

$$C_i = \frac{2E_i}{k(k-1)} \tag{4}$$

where k is the number of neighbors of a generic node i, E_i is the number of existing connections between those, $k(k-1)/2$ being the maximum number of connections, or combinations, that can exist among k nodes. Notice that the clustering coefficient C_i is defined locally, and a *global* value, C_c, is derived upon averaging C_i over all the nodes that compose the graph. The character-

istic path length (Cpl) is defined as the average number of steps along the shortest paths for all possible pairs of network nodes. We shall call the minimum distance between a generic couple of nodes the *shortest path length* (Spl), which is expressed as an integer number of steps. With these premises, we show now how to calculate the Spl for a couple of nodes n_l and n_m. In A, $a_{l,i}$ and $a_{i,m}$ account for all the pairs of nodes which are connected to n_l and n_m respectively. The sum of $a_{l,i}$ and $a_{i,m}$ over all the nodes in A, is stored in a new matrix $A_2 = \sum a_{l,i}\, a_{i,m}$ for all the l and m and A_2 has the same dimension of A. Now multiplicate A_2 and A repeatedly $A_2 = A_2\, A$, until all the terms of A_2 are non-zero and those terms in position ij will be the Spl between node i and node j. Finally, the *characteristic path length* Cpl is calculated like the average of Spl over A_2. Once obtained the C_c and Cpl values, we defined a precise measure of 'small-world-ness', the '*small-world-ness' coefficient (SW)*, based on the trade off between high local clustering and short path length. A network G with n nodes and m edges is a small-world network if it has a similar path length but greater clustering of nodes than an equivalent Erdos-Rényi (*E–R*) random graph with the same m and n (an *E–R* graph is constructed by uniquely assigning each edge to a node pair with uniform probability)[13,22]. Let Cpl_u and Cc_u be the mean shortest path length and the mean clustering coefficient for the *E–R* random graphs, obtained meaning the Cpl and the Cc of 20 uniform distributions, and Cpl_{graph} and Cc_{graph} the corresponding quantities for the graphs derived using the methods described above. We can calculate:

$$\gamma = \frac{Cc_{graph}}{Cc_u}$$
$$\lambda = \frac{Cpl_{graph}}{Cpl_u} \tag{5}$$

Thus, the *'small-worl-dness' coefficient* is

$$\mathrm{SW} = \frac{\gamma}{\lambda} \tag{6}$$

The categorical definition of small-world network above implies $\lambda \geq 1$, $\gamma \gg 1$ which, in turn, gives $\mathrm{SW} > 1$.

References

1 Bassett, D. S. & Bullmore, E. Small-World Brain Networks. *Neuroscientist* **12**, 512-523 (2006).
2 Bullmore, E. & Sporns, O. The economy of brain network organization. *Nature Reviews Neuroscience* **13**, 336-349 (2012).
3 Fano, U. A common mechanism of collective phenomena. *Reviews of Modern Physics* **64**, 313 (1992).
4 Hopfield, J. J. Neural networks and physical systems with emergent collective computational abilities. *Proc. Nat. Acad. Sci. USA* **79**, 2554-2558 (1982).
5 Koch, C. & Laurent, G. Complexity and the Nervous System. *Science* **284**, 96-98 (1999).
6 Melnattur, K. *et al.* Multiple redundant medulla projection neurons mediate color vision in Drosophila. *Journal of Neurogenetics* **28**, 374-388 (2014).
7 Onesto, V. *et al.* Nano-topography Enhances Communication in Neural Cells Networks. *Scientific Reports* **7**, 1-13 (2017).
8 Ravasz, E. & Barabási, A.-L. Hierarchical organization in complex networks. *Physical Review E* **67**, 026112 (2003).
9 Trabesinger, A. H. Aggregation phenomena: Collective diversity. *Nature Physics* **12** (2016).
10 Barabási, A.-L. & Oltvai, Z. N. Network biology: understanding the cell's functional organization. *Nature Reviews Genetics* **5**, 101–113 (2004).
11 Rubinov, M. & Sporns, O. Complex network measures of brain connectivity: Uses and interpretations. *NeuroImage* **52**, 1059–1069 (2010).
12 Sporns, O. Structure and function of complex brain networks. *Dialogues Clinical Neuroscence* **15**, 247-262 (2013).
13 Strogatz, S. H. Exploring complex networks. *Nature* **410**, 268-276 (2001).
14 Sun, Y. *et al.* Self-Organizing Circuit Assembly through Spatiotemporally Coordinated Neuronal Migration within Geometric Constraints. *Plos ONE* **6**, e28156 (2011).
15 Barabási, A.-L. *Network Science*. (Cambridge University Press, 2016).
16 Chartrand, G. & Zhang, P. *A First Course in Graph Theory*. (Dover Publications, 2012).
17 Gunduz, C., Yener, B. & Gultekin, S. H. the Cell Graphs of Cancer. *Bioinformatics* **20**, 145-151 (2004).
18 van Steen, M. *Graph Theory and Complex Networks: An Introduction*. (Maarten van Steen, 2010).
19 Lago-Fernández, L. F., Huerta, R., Corbacho, F. & Sigüenza, J. A. Fast Response and Temporal Coherent Oscillations in Small-World Networks. *Physical Review Letters* **84**, 2578 (2000).
20 Latora, V. & Marchiori, M. Efficient Behavior of Small-World Networks. *Physical Review Letters* **87**, 198701 (2001).
21 Takahashi, N., Sasaki, T., Matsumoto, W., Matsuki, N. & Ikegaya, Y. Circuit topology for synchronizing neurons in spontaneously active networks. *Proc. Nat. Acad. Sci. USA* **107**, 10244–10249 (2010).
22 Watts, D. J. *Small Worlds: The Dynamics of Networks between Order and Randomness*. (Princeton University Press, 2003).
23 Watts, D. J. & Strogatz, S. H. Collective dynamics of 'small-world' networks. *Nature* **393**, 440-442 (1998).
24 Marinaro, G. *et al.* Networks of Neuroblastoma Cells on Porous Silicon Substrates Reveal a Small World Topology. *Integrative Biology* **7**, 184-197 (2015).

25 Onesto, V. *et al.* Cortical-like mini-columns of neuronal cells on zinc oxide nanowire surfaces. *Scientific Reports* **9**, 4021-4017 (2019).
26 Accardo, A. *et al.* Multiphoton Direct Laser Writing and 3D Imaging of Polymeric Freestanding Architectures for Cell Colonization. *Small* **13**, 1700621-1700611 (2017).
27 Guo, R. *et al.* Micro lens fabrication by means of femtosecond two photon photopolymerization. *Optics Express* **14**, 810-816 (2006).
28 Gentile, F. *et al.* Fractal Structure Can Explain the Increased Hydrophobicity of NanoPorous Silicon Films. *Microelectronic Engineering* **88**, 2537-2540 (2011).
29 Meza, L. R. *et al.* Resilient 3D hierarchical architected metamaterials. *Proceedings of the National Academy of Sciences USA* **112**, 11502-11507 (2015).
30 Fleck, N. A., Deshpande, V. S. & Ashby, M. F. Micro-architectured materials: past, present and future. *Proceeding of the Royal Society A* **466**, 2495–2516 (2010).
31 du Roure, O. *et al.* Force mapping in epithelial cell migration. *Proceedings of the National Academy of Sciences USA* **102**, 2390-2395 (2005).
32 Rodriguez, A. & Laio, A. Clustering by fast search and find of density peaks. *Science* **344**, 1492–1496 (2014).
33 Waxman, B. Routing of multipoint connections. *IEEE Journal on Selected Areas in Communications* **6**, 1617–1622 (1988).
34 Béduer, A. *et al.* Elucidation of the Role of Carbon Nanotube Patterns on the Development of Cultured Neuronal Cells. *Langmuir* **28**, 17363-17371 (2012).
35 Accardo, A. *et al.* Two-photon lithography and microscopy of 3D hydrogel scaffolds for neuronal cell growth. *Biomedical Physics & Engineering Express* **4**, 027009-027008 (2018).
36 Humphries, M. D. & Gurney, K. Network 'Small-World-Ness': A Quantitative Method for Determining Canonical Network Equivalence. *PLoS ONE* **3**, e0002051 (2008).
37 Moore, C. & Newman, M. E. J. Epidemics and percolation in small-world networks. *Physical Review E* **61**, 5678 (2000).
38 Cossell, L. *et al.* Functional organization of excitatory synaptic strength in primary visual cortex. *Nature* **518**, 399-403 (2015).
39 Takahashi, N., Sasaki, T., Usami, A., Matsuki, N. & Ikegaya, Y. Watching neuronal circuit dynamics through functional multineuron calcium imaging (fMCI). *Neuroscience Research* **58**, 219–225 (2007).
40 Ercsey-Ravasz, M. *et al.* A Predictive Network Model of Cerebral Cortical Connectivity Based on a Distance Rule. *Neuron* **80**, 184-197 (2013).
41 Thiele, C. J. in *Human Cell Culture* Vol. 1 (ed Masters) 21-53 (Kluwer Academic Publishers, 1998).
42 Dorkenwald, S. *et al.* Automated synaptic connectivity inference for volume electron microscopy. *Nature Methods* **14**, 435–442 (2017).
43 Stetter, O., Battaglia, D., Soriano, J. & Geisel, T. Model-Free Reconstruction of Excitatory Neuronal Connectivity from Calcium Imaging Signals. *PLoS Computational Biology* **8**, e1002653 (2012).
44 von Bartheld, C. S., Bahney, J. & Houzel, S. H. The search for true numbers of neurons and glial cells in the human brain: A review of 150 years of cell counting. *Journal of Comparative Neurology* **524**, 3865-3895 (2016).

Figure Captions

Figure 1. The scaffold for cell culture growth and organization is a 3D network of regularly spaced polymeric cylinders (a), where the size and spacing of the cylinders is in the micro-meter range (b). Due to the fabrication process characteristics, the final structures are discretized into blocks with a lateral step size of $200\ nm$ (c). The surface roughness resulting from a similar step size is approximately $20\ nm$ – we have recreated the surface topography of the scaffold cylinder with a similar value of surface roughness (d). The power spectrum associated to the structures can be used the derive the fractal dimension of the scaffold - $D_f \sim 2.7$. High value of D_f reveals that the final prototype has details over multiple scales (e).

Figure 2. Light sheet microscopy enables to derive qualitative representation of cell distribution in the scaffold (a). Scanning electron microscopy of the cells suggest that their behavior and organization is guided by the nanometric details on the surface of the scaffolds (b, c).

Figure 3. Two photon microscopy was employed for precise, quantitative localization of cells within the volume of the scaffold (a). Front (a), side (b) and top (c) views of the scatter plot of the cells reveal that cells are unevenly distributed in the scaffold.

Figure 4. From the position of the cells within the volume of the scaffold (i.e. a cube), we derived the density distribution of cells projected onto either the lateral surfaces and the edges of the cube. Variations of the values of frequency are indicative of the non-uniformity of cells within the scaffold. Values of local density vary up to three times within the considered volume.

Figure 5. Unsupervised cluster analysis of cells (a) enabled to estimate the cluster centers in the originating distribution of cells (b) and attribute cells to specific clusters (c). Cluster centers are highlighted in the original distribution of cells.

Figure 6. To determine the topological parameters of cell distributions, cells were wired using the Waxman algorithm, using different probabilities of wiring.

Figure 7. After cell wiring (a) we determined the topological parameters of the networks as a function of the connectivity q. The degree of the network increases with the cubic power of q (b). Values of the clustering coefficient, cc, (c) and the characteristic path length, cpl, (d) are above 0.7 (cc) and below 3.5 (cpl) for large intervals of q. The small world coefficient is greater than one for any $q > 0.7$, indicating that cell networks exhibit small world characteristics (e).

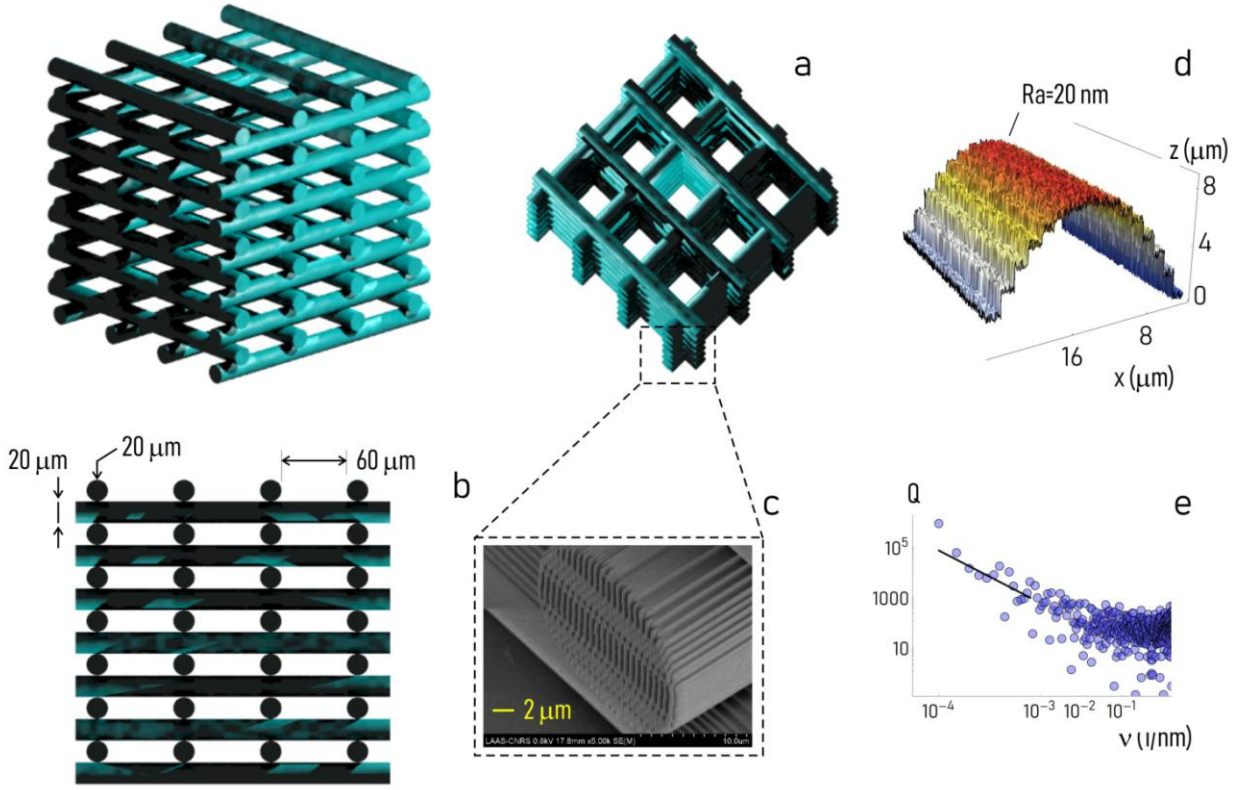

Figure 1

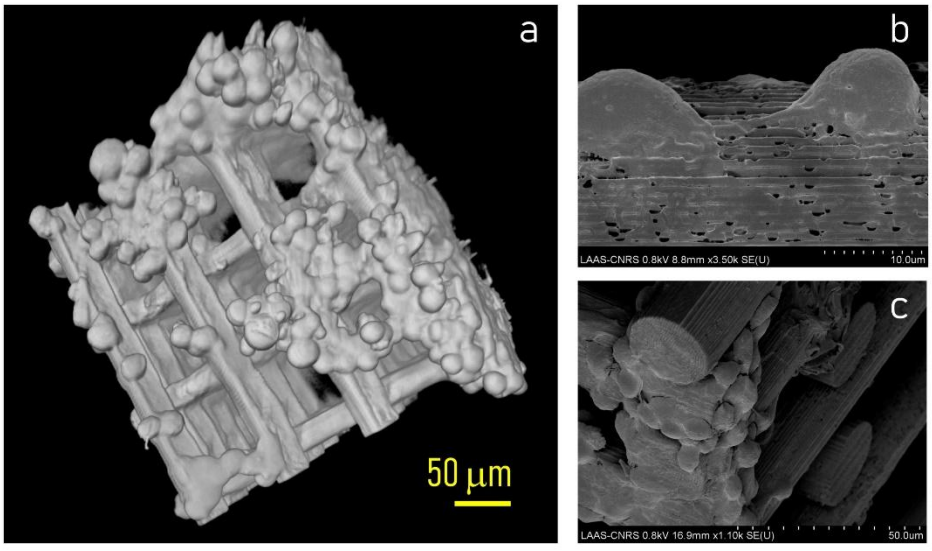

Figure 2

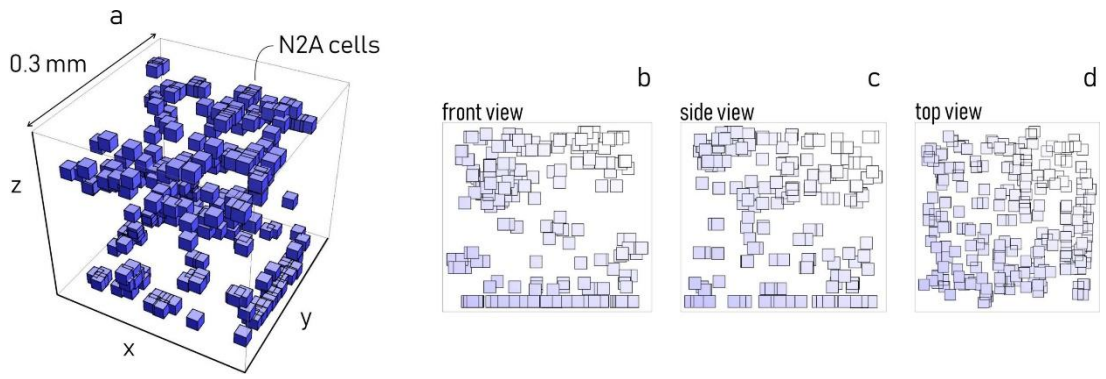

Figure 3

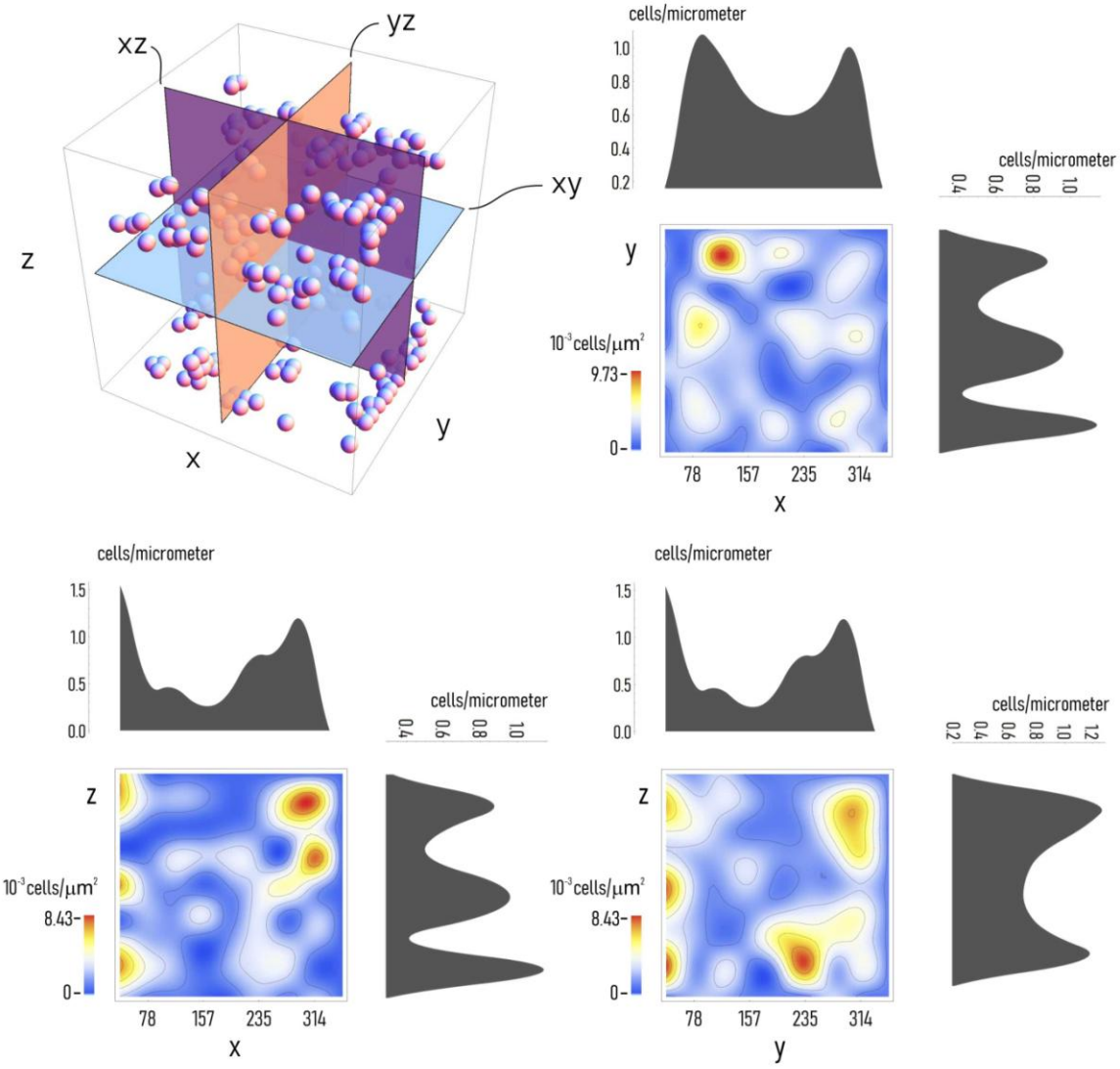

Figure 4

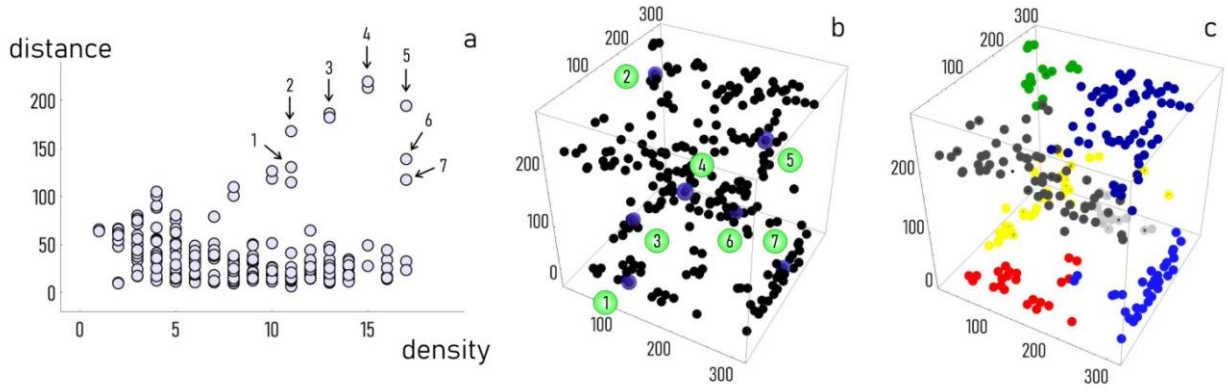

Figure 5

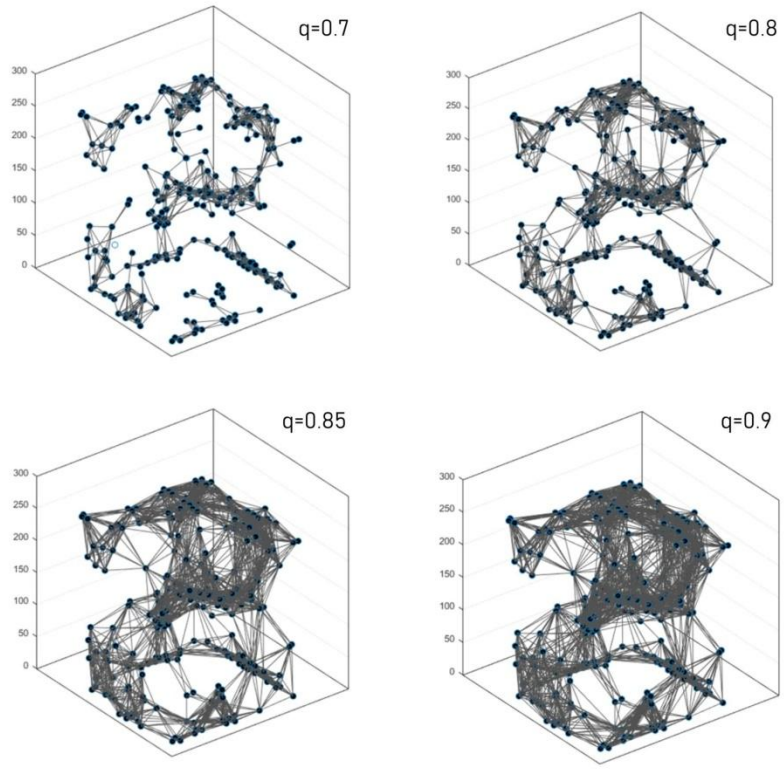

Figure 6

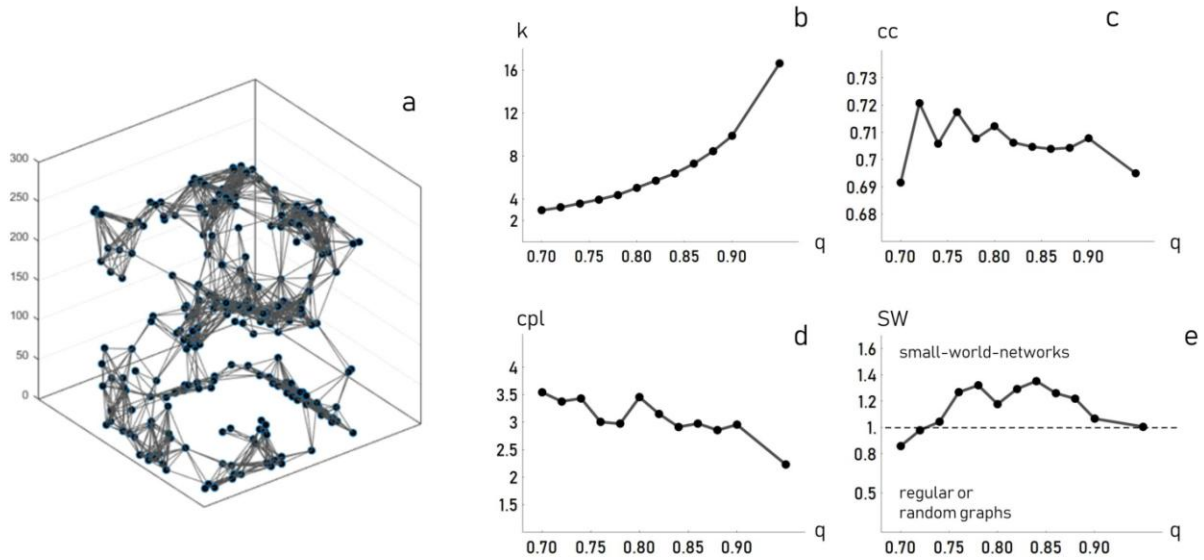
a
300
250
200
150
100
50
0
k
b
16
12
8
4
2
0.70 0.75 0.80 0.85 0.90
q
cc
c
0.73
0.72
0.71
0.7
0.69
0.68
0.70 0.75 0.80 0.85 0.90
q
cpl
d
4
3.5
3
2.5
2
1.5
0.70 0.75 0.80 0.85 0.90
q
SW
e
small-world-networks
1.6
1.4
1.2
1.
0.8
0.5
regular or
random graphs
0.70 0.75 0.80 0.85 0.90
q

Figure 7